JACS
JOURNAL OF THE AMERICAN CHEMICAL SOCIETY
pubs.acs.org/JACS
Article

# Catassembly Triad: A Catalytic Framework for Enantioselective Chiral Molecular Assembly

Zhihao Li,[⊥] Xuehai Huang,[⊥] Yansong Jiang, Wei Zeng, Ding Zou, Xue Dong, Liulin Yang, Xiaoyu Cao,* Zhongqun Tian,* and Yu Wang*

Cite This: https://doi.org/10.1021/jacs.5c16840
Read Online
ACCESS | Metrics & More | Article Recommendations | Supporting Information

**ABSTRACT:** Chiral molecular assembly represents a frontier in creating life-inspired functional materials; yet, a predictive framework for its enantioselective catalysis remains elusive. Here, we introduce the Catassembly Triad − a mechanistic paradigm for catalytic enantioselective assembly, demonstrated using chiral supramolecular cages as a model system. Combining in situ characterization, *ab initio* calculations, and machine learning, we resolve how catalysts must harmonize attachment, chiral control, and detachment to direct assembly pathways. Kinetic and structural analyses reveal that chiral diamine catalysts (e.g., cyclohexanediamine) enforce enantioselectivity by templating transient intermediates with deformation-induced affinity changes driving timely catalyst release. We establish a predictive framework based on quantitative triad metrics ($\Delta E_{att}$, $\Delta E_{ctl}$, and $\Delta E_{det}$) from calculations, validated by Bayesian clustering and experimental testing. The framework achieves a perfect concordance between predicted and observed catalyst efficacy across diverse molecular classes. This framework bridges enzymatic cooperativity and supramolecular assembly, enabling programmable chirality transfer and unlocking catalyst design for adaptive chiral materials.

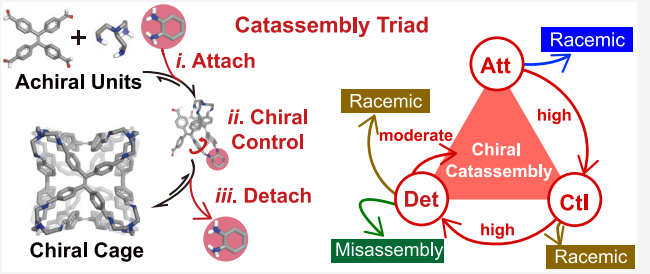


## INTRODUCTION

Chirality, from molecular synthesis to supramolecular assembly, lies at the heart of life's origins and modern functional materials. The transfer and amplification of chirality in molecular and supramolecular systems not only offer clues to prebiotic self-organization[1,2] but also underpin transformative applications in enantioselective catalysis,[3−5] chiral sensing,[6,7] and therapeutic delivery.[8] Over the past five decades, enantioselective catalysis at the molecular level has been revolutionized by Nobel-recognized advances, e.g., catalytic asymmetric synthesis[9−11] and asymmetric organocatalysis.[3,4] This progress has been driven by robust frameworks for catalyst design,[12−14] kinetic analysis,[15,16] and computational modeling of transient intermediates.[17,18]

Yet, extending enantioselective control to supramolecular assembly − a process critical to both life's emergence and programmable materials, remains a formidable challenge. While enantioselective chiral molecular assembly (ECMA) has enabled breakthroughs in synthetic biology[19−21] and chiral nanomaterials,[22−25] its catalytic control lags far behind molecular catalysis. Unlike well-defined molecular transformations, ECMA involves dynamic, multistep pathways where chirality emerges from cooperative interactions among transient intermediates.[26−29] This complexity renders conventional strategies inadequate in studying catalytic assembly (i.e., catassembly[30]): (1) in situ characterization struggles to resolve complex assembly pathways;[31,32] (2) theoretical methods face limitations in modeling large supramolecules or infinite systems;[33−35] and (3) design principles for stereochemical amplification in assemblies remain empirical.[36−39] Consequently, a predictive mechanistic framework for catalytic ECMA has yet to emerge.

Here, we bridge this gap by introducing the Catassembly Triad: a catalytic framework for ECMA. Using chiral supramolecular cages as a model system, we integrate in situ characterization, theoretical calculations, and machine learning (ML) to establish a predictive platform for catalyst design. The triad identifies three synergistic principles (attach, control, and detach) as essential for effective catalytic ECMA and delivers an ML-driven computational pipeline to measure catalyst efficacy. This framework resolves persistent mechanistic ambiguities in catalytic assembly[40] and establishes generalizable design rules for stereochemical amplification in supramolecular systems.

## RESULTS AND DISCUSSION

**Catalytic Enantioselective Assembly: Model System and Research Framework.** For over a decade, our team has

Received: September 24, 2025
Revised: December 10, 2025
Accepted: December 11, 2025

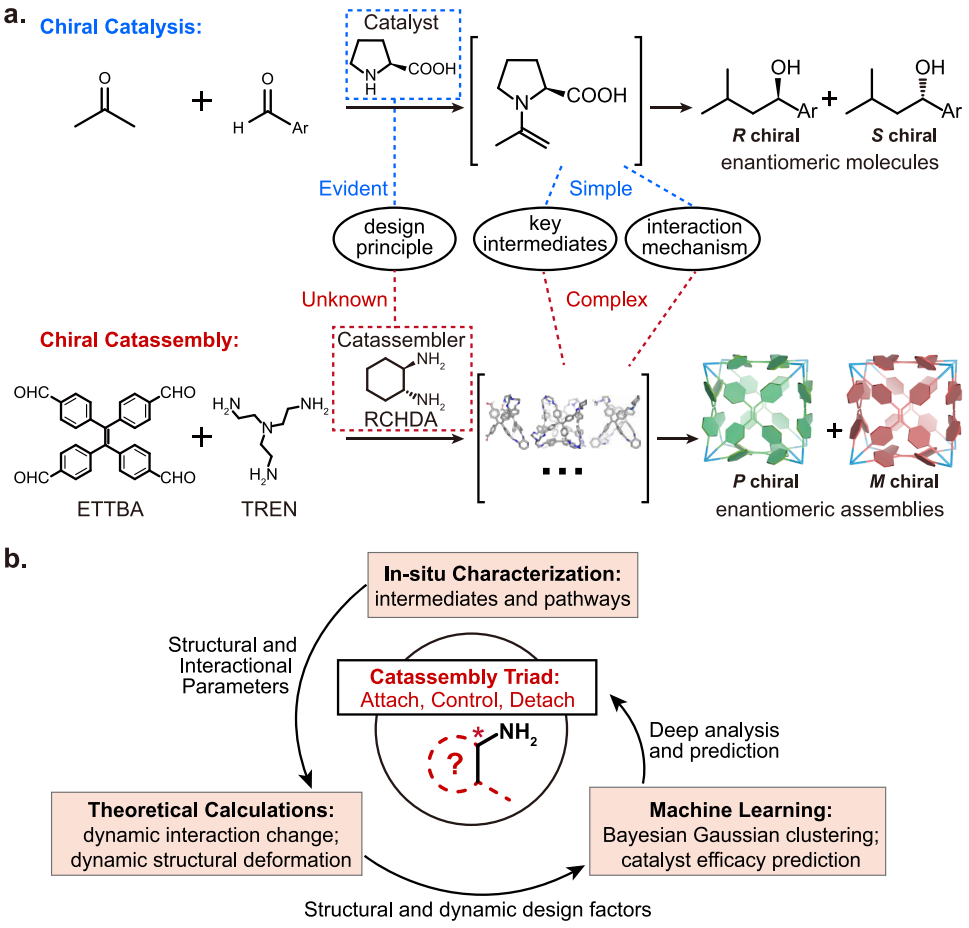


**Figure 1.** Conceptual framework for catalytic enantioselective molecular assembly. (a) Comparative complexity of classical organocatalysis (Benjamin List reaction) versus catalytic molecular assembly (catassembly) in supramolecular cages, highlighting differences in design principles, intermediate characterization, and mechanistic understanding. (b) Integrated research pipeline establishing the Catassembly Triad framework through in situ characterization, theoretical calculations, and machine learning.

developed catassembly (catalytic assembly) concepts to advance supramolecular systems with the same transformative impact that catalysis has brought to chemical synthesis.[30,40−43] While diverse catassembly systems (e.g., supramolecular cages,[44−46] supramolecular polymers,[47−50] host−guest assemblies,[51] and DNA/peptide/nucleosome assemblies[52−56]) have demonstrated broad utility across materials science and biology, their design remains empirical, lacking a predictive mechanistic framework.

To establish such a framework, we focus on chiral supramolecular cages as a model system (Figure 1a). Their well-defined structures enable unambiguous intermediate identification; their discrete bonding facilitates reliable DFT calculations; and their strong chiroptical signatures permit quantitative tracking of enantioselective amplification. Yet even this "simplest" catassembly system exhibits staggering complexity compared with that of molecular catalysis. For instance, a prototypical organocatalytic reaction studied by Benjamin List (Figure 1a, top) involves one reaction site with well-defined intermediates via DFT calculations and ultrafast spectroscopy, enabling rational catalyst design. In stark contrast, our $[E]_6[T]_8$ cage system assembles from six 4,4′,4″,4‴-(ethene-1,1,2,2-tetrayl)tetrabenzaldehyde (ETTBA, [E] in formulas) and eight tris(2-aminoethyl)amine (TREN, [T] in formulas) subunits through 24 dynamic covalent bonds, generating diverse, transient intermediates with elusive interchange pathways (Figure 1a, bottom). Consequently, assembly catalyst (i.e., catassembler) design relies on trial and error − a universal limitation across complex molecular assembly.

Guided by experimental screening, we identified cyclohexanediamine (CHDA) as an effective catassembler (catalyst) for enantioselective cage formation (*P*/*M* chirality). To decode its function, we integrated three methodologies (Figure 1b): in situ characterization (real-time monitoring of intermediates), density functional theory (DFT) calculations (energy landscape mapping), and machine learning (catalyst efficacy prediction). This pipeline revealed the Catassembly Triad: three synergistic principles − attach, control, and detach − that are essential for efficient catalytic enantioselective assembly.

**Chirality Control through Catalytic Assembly.** Building on prior structural characterization of the $[E]_6[T]_8$ cage system (Figure S1)[57] via single-crystal X-ray diffraction (XRD), mass spectrometry (MS), high-performance liquid chromatography (HPLC), and circular dichroism (CD) spectroscopy, we now demonstrate that introducing CHDA catalytically drives enantioselective cage formation. (*R*,*R*)- or (*S*,*S*)- CHDA lead to the *P*- or *M*-riched enantiomeric excess of cage products, respectively, showing mirror-image CD spectra (Figure S2). Control experiments using racemic CHDA (Figure S3) lead to no CD signal, confirming that the formation of enantiomerically enriched cages is indeed determined by the absolute configuration of the chiral catalyst, and not by any spontaneous


https://doi.org/10.1021/jacs.5c16840
J. Am. Chem. Soc. XXXX, XXX, XXX−XXX

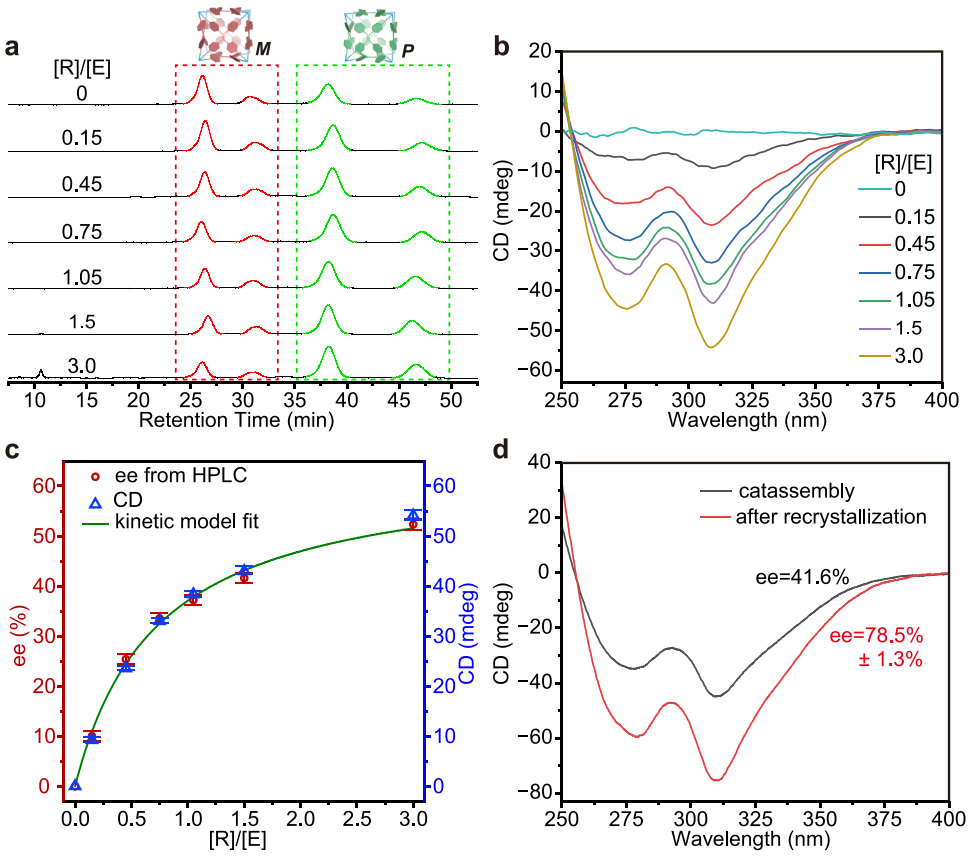


**Figure 2.** Enantioselective control in catalytic assembly. (a) Chiral HPLC traces of $[E]_6[T]_8$ cages at varying RCHDA concentrations. (b) Circular dichroism (CD) spectra showing chiroptical amplification upon the increase of RCHDA. (c) Enantiomeric excess derived from HPLC (circles) and CD (triangles) versus RCHDA concentration, with kinetic model fit (green line). (d) Enantiomeric excess enhancement from 41.6% to 78.5% via single recrystallization.

symmetry breaking. Crucially, CHDA acts as a true catalyst: MS confirms $[E]_6[T]_8$ formation with no CHDA adducts (Figure S4). Due to the symmetric nature of (*R*,*R*)- and (*S*,*S*)-CHDA, we use (*R*,*R*)-CHDA as the default CHDA to perform experimental and computational studies and abbreviate it as RCHDA or [R] in formulas.

Competition between the RCHDA-catalyzed assembly and background self-assembly governs enantioselectivity. Increasing the RCHDA/TREN ratio enhances enantiomeric excess (ee) toward *P*-enriched cages (Figure 2a, HPLC) and amplifies the negative Cotton effect of CD signals (Figure 2b). HPLC and CD data quantitatively correlate with each other (Figure 2c) with a coefficient of $R^2 > 0.99$ (Figure S5), and together they reveal a nonlinear dependence of ee on catalyst loading.

To ascribe this nonlinear effect to the pathway competition between catalyzed assembly and self-assembly, we derive a kinetic model assuming pseudo-first-order rate constants (see SI for details): $k_c$ for the RCHDA-catalyzed pathway and $k_s$ for TREN-mediated self-assembly. The enantiomeric excess follows:

$$\text{ee} = \frac{\alpha \cdot c(\text{RCHDA})}{c(\text{RCHDA}) + \beta \cdot c(\text{TREN})}, \qquad \beta = \frac{k_s}{k_c} \tag{1}$$

where $\alpha$ represents the chiral control efficiency of RCHDA; $\beta$ represents the relative reactivity of TREN versus RCHDA; $c$(RCHDA) and $c$(TREN) represent the initial concentrations of RCHDA and TREN, respectively. Experimental ee values fit this model with $\alpha = 0.64$, $\beta = 0.73$, and $R^2 > 0.99$. We intentionally selected this system — where self-assembly and catalyzed assembly coexist ($\beta = 0.73$, limiting ee to 41.6% at $c$(RCHDA)/$c$(TREN) = 1.5) to amplify intermediate concentrations for mechanistic studies.

Note that, due to the complexity of pathways illustrated later in Figure 3, this simple two-pathway competition model cannot capture the multistep reality where catalyst incorporation, progressive displacement, and final release occur as distinct processes. The parameters $\alpha$ and $\beta$ are, therefore, empirical fitting constants rather than fundamental rate constant ratios.

**Post-Assembly Chirality Enhancement.** The catalytic assembly provides a foundational enantiomeric excess, which can be further enhanced through physical and catalytic recycling strategies. A single recrystallization of the thermodynamic product consistently increased the ee from 41.6% to 78.5 ± 1.3% in the mother liquor (Figure 2d). This amplification arises from a physical separation process and not a chemical transformation. As schematized in Figure S6, the racemic (*P*/*M*) pair of cages exhibits a higher propensity to cocrystallize than enantiopure pairs. Consequently, the solid precipitate is enriched in the racemic compound, thereby selectively concentrating the desired *P*-enantiomer in the solution phase and providing a practical route to a high-ee material from a catalytically enriched mixture.

The catalytic nature of RCHDA, which is crucial for this strategy, is unambiguously confirmed by quantitative NMR and recyclability tests. NMR analysis with an internal standard verified that over 99% of the RCHDA catalyst remains in a


https://doi.org/10.1021/jacs.5c16840
J. Am. Chem. Soc. XXXX, XXX, XXX−XXX

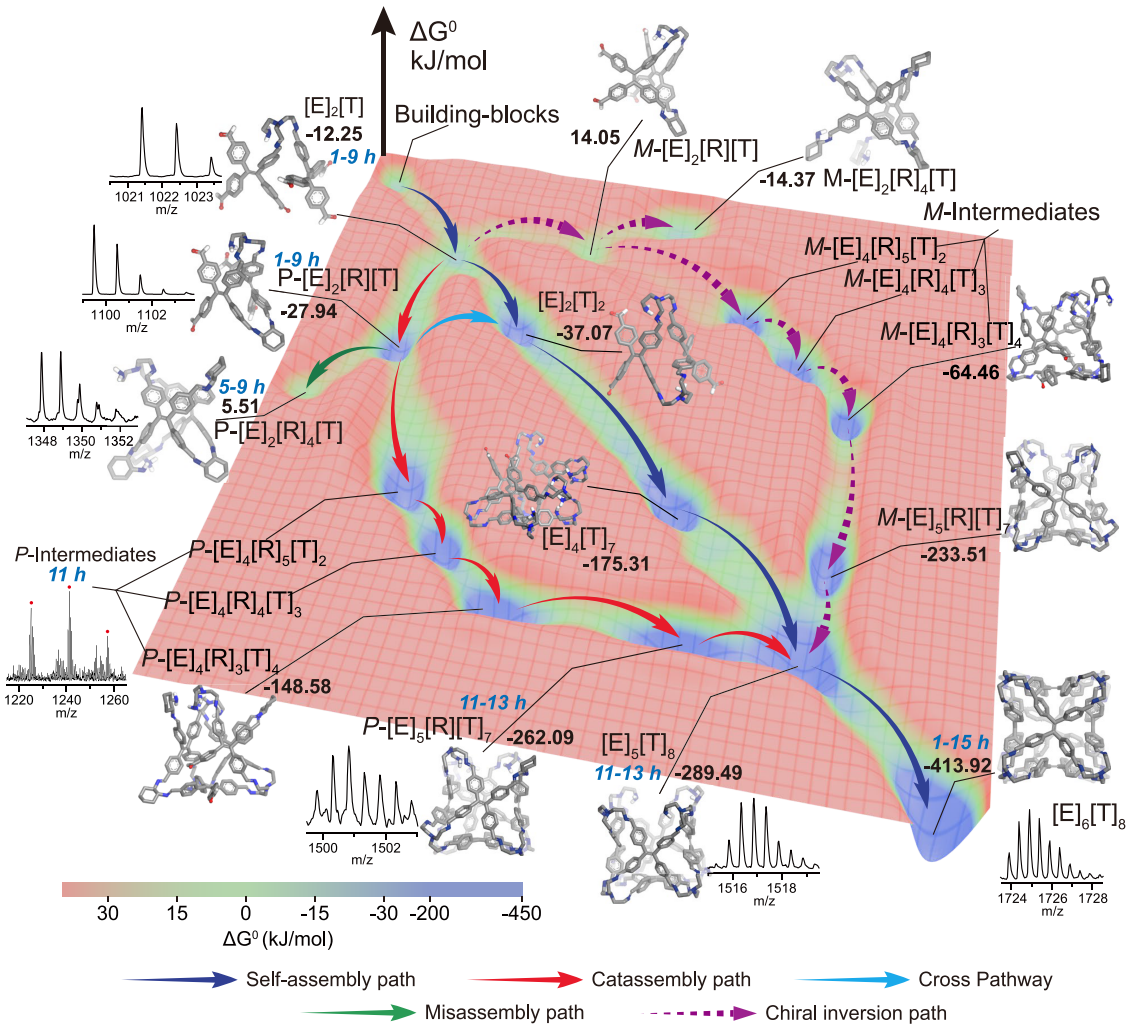


**Figure 3.** Energy landscapes and pathways in catalytic assembly. Gibbs free energy surface computed via DFT calculation for intermediates identified by in situ mass spectrometry. Pathways are color-coded: self-assembly (blue), catassembly (red), cross-pathways (cyan), misassembly (green), and chiral inversion (purple). Insets: Optimized structures, calculated energies, and mass spectra of key intermediates.

dissociative state in the final product, ruling out stoichiometric incorporation (Figure S7). Furthermore, the catalyst demonstrated excellent recyclability. Upon adding a second equivalent of building blocks to the postreaction mixture, the ensuing assembly cycle produced cages with nearly identical enantiomeric excess (~42%) and doubled CD intensity (Figure S8), confirming that RCHDA retains its stereochemical control over multiple catalytic turnovers.

**Intermediates and Pathways Revealed via *In Situ* Characterization and DFT Calculations.** We developed an in situ MS methodology to monitor the formation and evolution of assembly intermediates in real time. Figures 3 and S9−S11 depict representative intermediates with their mass spectra and temporal profiles, enabling reconstruction of both self-assembly and catassembly pathways. Beyond capturing self-assembly intermediates and their straightforward progression from $[E]_2[T]$ to $[E]_6[T]_8$, we identified critical catalytic steps: (1) Beginning as early as 1 h and persisting through the first 9 h, RCHDA attaches to $[E]_2[T]$ to form $[E]_2[R][T]$, initiating chirality transfer; (2) Progressively over time and culminating between 11 and 13 h, gradual displacement of RCHDA by TREN occurs via transitions through $[E]_4[R]_5[T]_2 \rightarrow [E]_4[R]_4[T]_3 \rightarrow [E]_4[R]_3[T]_4$; (3) Emerging by 11 h and continuing until completion, RCHDA release from $[E]_5[R][T]_7$ yields $[E]_5[T]_8$, culminating in the final cage. Transient misassembled intermediates (e.g., $[E]_2[R]_4[T]$) disappear in the products, demonstrating error correction through dynamic bond exchange.

Recognizing the qualitative nature of electrospray ionization MS (ESI-MS) and potential ionization efficiency effects, we performed additional validation. Measurement of a controlled 1:1:1 mixture of $[E]_1[R]_4$, $[E]_3[R]_6$, and $[E]_6[T]_8$ showed comparable peak abundances (Figure S12), confirming that ionization efficiencies, while not identical, do not invalidate the relative trends observed in time-resolved studies. Thus, the pathway $[E]_2[T] \rightarrow [E]_2[R][T] \rightarrow [E]_4[R]_3[T]_4 \rightarrow [E]_5[R][T]_7 \rightarrow [E]_5[T]_8$ represents a mechanistically relevant route, although not necessarily exclusive.

Furthermore, isotope labeling experiments in $CDCl_3$ with 1% $D_2O$ revealed increased D,D-labeled [R] over time (Figure S13), directly evidencing deuterium incorporation during imine-bond hydrolysis in the catalyst detachment step. This provides independent confirmation of the dynamic attachment/detach catalytic cycle.

DFT calculations mapped energy landscapes by using the intermediates identified experimentally. Figure 3 shows the


https://doi.org/10.1021/jacs.5c16840
J. Am. Chem. Soc. XXXX, XXX, XXX−XXX

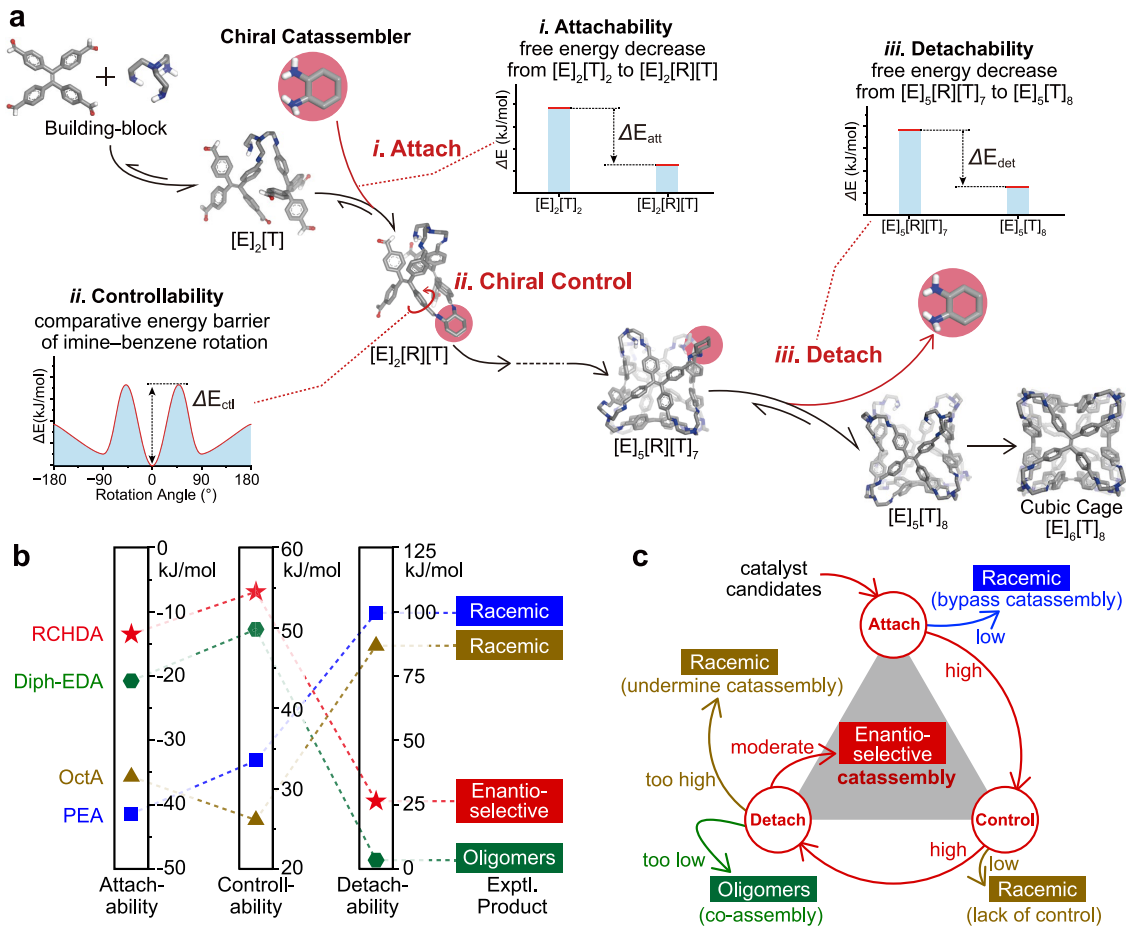


**Figure 4.** Quantitative metrics of the Catassembly Triad. (a) Triad schematic defining key factors – attachability ($\Delta E_{att}$), controllability ($\Delta E_{ctl}$), and detachability ($\Delta E_{det}$) – with computational quantification methods. (b) Calculated triad metrics for RCHDA versus control amines (Diph-EDA, OctA, and PEA), correlated with experimental analysis of product chirality. (c) Triad efficacy principles derived from panel (b): high attachability/controllability with moderate detachability enables effective enantioselective catalyzed assembly.

calculated energies of all intermediates along with their optimized structures. Both self-assembly and catassembly pathways exhibit cascading energy decreases, demonstrating each step of transformation is thermodynamically favorable, and explaining their coexistence as observed experimentally. In contrast, *M*-configured intermediates show substantially higher energies (e.g., $\Delta\Delta G$ = 42 kJ/mol for $[E]_2[R][T]$), suggesting *P*-configuration dominance within the catassembly pathway. In addition, the misassembled species showed >30 kJ/mol higher formation energies, rationalizing their disappearance.

Critically, the similar formation energies of $[E]_2[R][T]$ and $[E]_2[T]_2$ ($\Delta\Delta G \approx 9$ kJ/mol) enables a feasible "cross-pathway" (cyan arrow, Figure 3) where [T] displaces [R] from *P*-$[E]_2[R][T]$, regenerating $[E]_2[T]_2$. This pathway explains why ~36% of *P*-$[E]_2[R][T]$ population leaks back to the racemic self-assembly pool (consistent with $\alpha$ = 0.64 from eq 1), despite the high intrinsic stereochemical preference. This phenomenon highlights a key feature of complex molecular assembly: its gentle energy landscape allows multiple pathways to coexist and compete kinetically.[58]

**Kinetics of the Competing Pathways.** To elucidate the dynamic competition among pathways, we performed time-resolved UV–vis spectroscopy. As shown in Figure S14, the self-assembly and catassembly processes exhibit distinct kinetic profiles. The self-assembly pathway progresses through a slow, multistage process characterized by an initial absorbance increase at 365 nm (attributable to early intermediates like $[E]_2[T]_2$), followed by a gradual spectral shift to signatures of larger intermediates and the final cage (increases at 307/314 nm). In stark contrast, the RCHDA-catalyzed pathway is markedly accelerated, exhibiting rapid spectral changes across all characteristic wavelengths within 0.5 h and reaching completion by ~8 h.

These kinetic data provide direct evidence that the RCHDA catalysis effectively accelerates the assembly process. The spectral evolution patterns are consistent with the coexistence and competition between multiple pathways, as depicted in the energy landscape (Figure 3). Temperature-dependent studies further reveal that the product enantiomeric excess remains essentially constant across temperatures (Figure S15), indicating that the effective $\Delta\Delta G$ governing the enantioselective outcome is small (on the order of RT, ~3 kJ/mol). This value aligns with both the empirical parameter $\alpha$ from our kinetic model and the energy barrier of the identified "cross-pathway", confirming that the net enantioselection is governed by kinetic competition between pathways with similar energy barriers.

**Catassembly Triad: A Predictive Framework for Catalytic Assembly.** Analysis of the catalytic pathway reveals that effective catalysts must execute three harmonized processes: attachment to assembly intermediates, chiral control during growth, and timely detachment – collectively termed the Catassembly Triad. Using RCHDA as a model system, we


https://doi.org/10.1021/jacs.5c16840
J. Am. Chem. Soc. XXXX, XXX, XXX−XXX

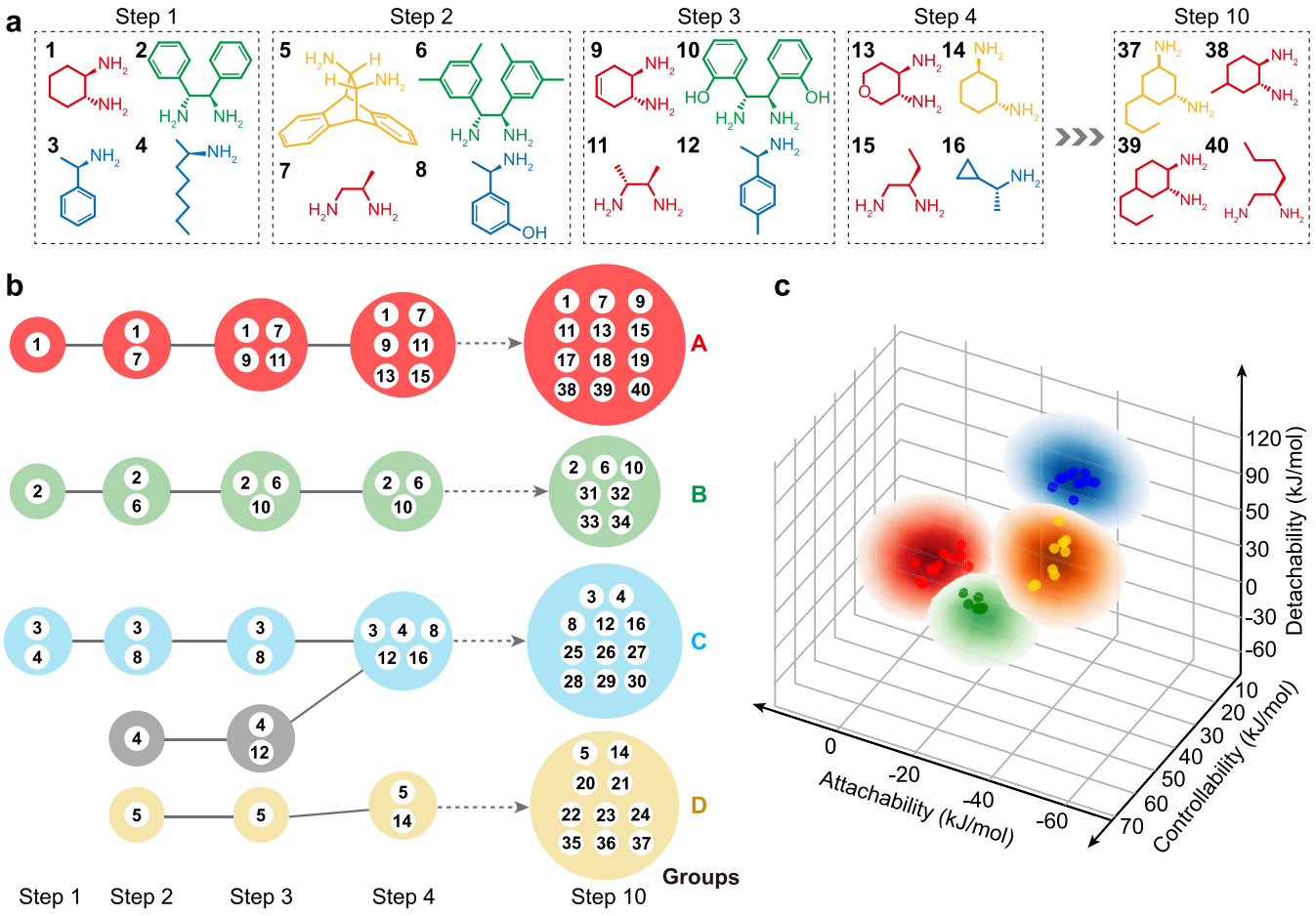


**Figure 5.** Machine-learning prediction of catalyst efficacy. (a) Structures of 40 catalyst candidates used in 10 iterations of a clustering model. (b) Cluster evolution during iterative Bayesian Gaussian Mixture Model (BGMM) refinement. (c) 3D probability map of catalyst classification based on triad metrics, generated via Gaussian Process regression. Opacity indicates prediction confidence.

established a predictive framework to provide a quantitative basis for categorical prediction by evaluating triad metrics through theoretical simulation of key intermediates identified via in situ experiments (Figure 4a).

- Attachability is defined as the energy decrease upon forming the initial catalyst-bound intermediate $[E]_2[R][T]$ relative to its self-assembly counterpart $[E]_2[T]_2$:

$$\Delta E_{att} = \Delta E_{[E]_2[T]_2} - \Delta E_{[E]_2[R][T]}$$

- Controllability ($\Delta E_{ctl}$) was defined as the activation energy barrier for imine-benzene bond rotation in the key intermediate $[E]_2[C][T]$, representing the energy required for chiral inversion (Figure S16).
- Detachability is defined as the energy decrease upon catalyst release from $[E]_5[R][T]_7$ via TREN substitution:

$$\Delta E_{det} = \Delta E_{[E]_5[T]_8} - \Delta E_{[E]_5[R][T]_7}$$

Greater values of $\Delta E_{att}$, $\Delta E_{ctl}$, or $\Delta E_{det}$ correspond to higher attachability, controllability, and detachability, respectively. To ensure accuracy and consistency, we implemented a unified and benchmarked xTB//M06-2X hybrid protocol for calculating all three Triad metrics (Supplementary Methods).

Figure 4b compares the calculated triad metrics for RCHDA, (*R*,*R*)-1,2-diphenylethanediamine (Diph-EDA), (*R*)-2-octylamine (OctA), and (*R*)-1-phenethylamine (PEA), correlated to their experimental outcomes. RCHDA exhibits synergistic metrics: high attachability ($\Delta E_{att}$ = −12.8 kJ/mol), high controllability ($\Delta E_{ctl}$ = 54.6 kJ/mol), and moderate detachability ($\Delta E_{det}$ = 27.2 kJ/mol) enable effective enantioselective catalysis. Comparative analysis of alternative candidates confirms that deficiencies in any triad component universally impair catalytic function:

- Weak attachability in PEA ($\Delta E_{att}$ = −42.1 kJ/mol) prevents catalyst binding against TREN competition, yielding racemic products.
- Weak controllability in OctA ($\Delta E_{ctl}$ = 26.3 kJ/mol) underperforms even TREN's chiral control, yielding racemic products.
- Poor detachability of Diph-EDA ($\Delta E_{det}$ = 4.5 kJ/mol) traps assembly in coassembly pathways, forming noncage oligomers.

These results establish qualitative efficacy principles (Figure 4c): high attachability/controllability with moderate detachability enables effective enantioselective catalysis.

An effective catalyst must strike a balance between strong initial binding and timely release − a dynamic interaction essential for catalytic function and triad harmony. Structural analysis (Figure S17) reveals this behavior stems from dynamic deformation:


https://doi.org/10.1021/jacs.5c16840
J. Am. Chem. Soc. XXXX, XXX, XXX−XXX

**Table 1. Experimental Validation of Nine Representative Catalyst Candidates**

| Catalyst Candidate | Group | No. | Self-detach | Chiral induction |
|---|---|---|---|---|
| 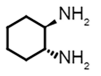 | A | **1** | ✓ | ✓ |
| 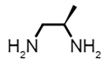 | A | **7** | ✓ | ✓ |
| 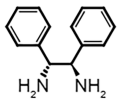 | B | **2** | × | No Cage Product |
| 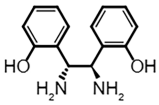 | B | **10** | × | No Cage Product |
| 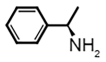 | C | **3** | ✓ | × |
| 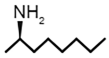 | C | **4** | ✓ | × |
|  | C | **16** | ✓ | × |
|  | D | **14** | ✓ | × |
| 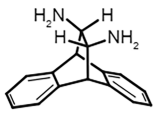 | D | **5** | ✓ | × |

- Early intermediates ($[E]_2[T]$ and $[E]_2[R][T]$) show minimal imine distortion ($\Delta\theta < 0.5°$), enabling flexible catalyst attachment.
- Added building blocks increase rigidity in latter stage intermediates (e.g., $[E]_5[R][T]_7$), amplifying distortion ($\Delta\theta > 1.2°$) and driving RCHDA release.
- Following release, the distortion relaxes in $[E]_5[T]_8$ and in the final cage $[E]_6[T]_8$.

The imine distortion serves as a representative metric of broader structural strain, whereas the total energy difference driving catalyst release arises from cumulative deformations including imine-bond angles, benzene dihedral angles, and other bond distortions. This deformation-induced affinity modulation resembles enzyme−substrate dynamics,[59] revealing mechanistic unity across catalytic regimes.

**Machine-Learning-Assisted Analysis of the Triad Theory.** To validate the Catassembly Triad framework, we implemented a variational Bayesian Gaussian Mixture Model (BGMM)[60−62] that clusters catalyst molecules based on three key descriptors: attachability, controllability, and detachability. This Bayesian approach autonomously determines optimal cluster numbers while quantifying uncertainty − a critical advantage for avoiding overfitting with limited data sets. Beginning with RCHDA and control molecules from Figure 4, we iteratively expanded our data set to 40 samples over 10 stages (Figure 5a). Figure 5b visualizes the evolving cluster assignments during sequential sample addition, revealing how classifications merge and split during model refinement. After 10 iterative rounds of optimization, the model converged on a stable classification of four distinct categories (down from an intermediate state of five). The model's convergence, monitored by the Evidence Lower Bound (ELBO, as depicted in Figure S18), demonstrated robustness despite a temporary fluctuation when the new functional groups were introduced, ultimately falling below the threshold after eight iterations.

Classification confidence was visualized through a 3D probability map (Figure 5c), generated via Gaussian Process (GP) regression[60,63] with radial basis function (RBF) kernel:

$$k(x_i, x_j) = \exp\left(-\frac{d(x_i, x_j)^2}{2l^2}\right) \quad (2)$$

where $l$ is the kernel length scale and $d(x_i, x_j)$ is the Euclidean distance. This RBF kernel assumes smooth, infinitely differentiable functions − physically consistent with gradual energy changes during molecular assembly. The resulting probability visualization renders opacity-graded ellipsoidal regions with high-confidence core voxels transitioning to translucent surfaces in uncertain zones.

GP validation identified four distinct catalyst groups:

- Group A contains nonaromatic diamines with high attachability, high controllability, and moderate detachability. RCHDA and analogs occupy high-confidence central regions, predicting effective catalysis.
- Group B comprises aromatic diamines sharing the same skeleton containing two benzene rings. They show high controllability but poor detachability, suggesting coassembly traps.


https://doi.org/10.1021/jacs.5c16840
J. Am. Chem. Soc. XXXX, XXX, XXX−XXX

- Group C includes monoamines exhibiting low attachability and controllability due to lack of cooperative binding sites.
- Group D contains diamines with mismatched configuration or divergent dihedral angles, leading to low attachability and invalid modulations.

Experimental validation of nine representative catalyst candidates (Table 1) confirmed these predictions (Figures S19 and S20): Group A molecules (e.g., catalysts **1** and **7**) successfully implemented chirality without product incorporation; Group B molecules (e.g., **2** and **10**) formed oligomers that blocked cage formation, due to the low detachability; while Groups C and D catalysts (e.g., **3**, **4**, **16**, **14**, and **5**) failed chirality transfer due to low attachability or low controllability. This perfect alignment between computational prediction and experimental validation demonstrates the Catassembly Triad framework's predictive power for catalyst screening.

## CONCLUSIONS AND PERSPECTIVES

The Catassembly Triad bridges a fundamental gap in supramolecular science by providing a mechanistic framework for controlling enantioselective assembly without incorporating the catalyst into the final product. By deconstructing the process into three synergistic steps (attachment, control, and detachment), we establish a universal paradigm for catalytic assembly. Our interdisciplinary approach reveals that effective catalysts must:

- Exploit structural flexibility in early intermediates for chiral templating,
- Leverage rigidity-driven strain in late intermediates to trigger catalyst release, mirroring enzyme−substrate dynamics,
- Require a delicate balance among triad metrics, where imbalance leads to kinetic traps or racemization.

This work establishes the Catassembly Triad as a foundational, proof-of-concept framework that provides a quantitative basis for categorical prediction, transforming catalyst screening from an empirical endeavor to a rational design process.

Looking forward, the Triad principles show significant potential for applications beyond discrete imine cages. A qualitative retroactive analysis of the literature systems supports this generality. For instance, in the classic TPPS supramolecular polymer system, chiral amines act as coassemblers due to high attachability but poor detachability,[64] whereas chiral imine cages function as true catalysts by balancing moderate attachability, high controllability, and phase separation-driven detachability.[47] Furthermore, our preliminary work applying these principles to Metal−Organic Frameworks (MOFs) has already enabled the creation of functional materials inaccessible via conventional routes, highlighting the framework's broad utility and promising a separate, detailed study.

To fully realize the potential of predictive catalytic assembly, future work will focus on:

- Developing systematic experimental tools for resolving the kinetics of complex, multistep assembly pathways.
- Advancing computational methods, potentially through AI-acceleration, to achieve high accuracy for large, flexible supramolecular systems.
- Extending the framework to quantitatively predict enantiomeric excess (ee) by modeling the competition between all relevant pathways.
- Adapting and applying the Triad framework to diverse supramolecular systems − including peptides, DNAs, and MOFs − to generate functional chiral matter that is unattainable through self-assembly or coassembly.

By charting this course, we aim to bridge supramolecular and enzymatic complexity, unlocking a new era of programmable chiral materials.

## ASSOCIATED CONTENT

### Supporting Information

The Supporting Information is available free of charge at https://pubs.acs.org/doi/10.1021/jacs.5c16840.

Single-crystal X-ray structures and computed CD spectra; spectroscopic data (CD, UV−vis, NMR) of assembly and recrystallization products; mass spectrometry (time-resolved intermediates, isotope tracking, ionization efficiency, catalyst screening); computational energy landscapes, imine-bond rotation profiles, distortion analysis, and method benchmarks; machine-learning model convergence and 3D probability maps; experimental methods and data tables. (PDF)

## AUTHOR INFORMATION


### Corresponding Authors

**Xiaoyu Cao** − *State Key Laboratory of Physical Chemistry of Solid Surfaces and College of Chemistry and Chemical Engineering, Xiamen University, Xiamen 361005, China;* orcid.org/0000-0003-0219-1798; Email: xcao@xmu.edu.cn

**Zhongqun Tian** − *State Key Laboratory of Physical Chemistry of Solid Surfaces and College of Chemistry and Chemical Engineering, Xiamen University, Xiamen 361005, China;* orcid.org/0000-0002-9775-8189; Email: zqtian@xmu.edu.cn

**Yu Wang** − *South China Advanced Institute for Soft Matter Science and Technology, School of Emergent Soft Matter, South China University of Technology, Guangzhou 510640, China; Center for Electron Microscopy and Guangdong Provincial Key Laboratory of Functional and Intelligent Hybrid Materials and Devices, South China University of Technology, Guangzhou 510640, China*; Email: roywangyu@scut.edu.cn

### Authors

**Zhihao Li** − *South China Advanced Institute for Soft Matter Science and Technology, School of Emergent Soft Matter, South China University of Technology, Guangzhou 510640, China; State Key Laboratory of Physical Chemistry of Solid Surfaces and College of Chemistry and Chemical Engineering, Xiamen University, Xiamen 361005, China*

**Xuehai Huang** − *South China Advanced Institute for Soft Matter Science and Technology, School of Emergent Soft Matter, South China University of Technology, Guangzhou 510640, China*

**Yansong Jiang** − *South China Advanced Institute for Soft Matter Science and Technology, School of Emergent Soft Matter, South China University of Technology, Guangzhou 510640, China*

**Wei Zeng** − *State Key Laboratory of Physical Chemistry of Solid Surfaces and College of Chemistry and Chemical Engineering, Xiamen University, Xiamen 361005, China*




https://doi.org/10.1021/jacs.5c16840
J. Am. Chem. Soc. XXXX, XXX, XXX−XXX

**Ding Zou** − *State Key Laboratory of Physical Chemistry of Solid Surfaces and College of Chemistry and Chemical Engineering, Xiamen University, Xiamen 361005, China*
**Xue Dong** − *State Key Laboratory of Physical Chemistry of Solid Surfaces and College of Chemistry and Chemical Engineering, Xiamen University, Xiamen 361005, China*
**Liulin Yang** − *State Key Laboratory of Physical Chemistry of Solid Surfaces and College of Chemistry and Chemical Engineering, Xiamen University, Xiamen 361005, China;* orcid.org/0000-0003-3342-8137

Complete contact information is available at: https://pubs.acs.org/10.1021/jacs.5c16840

### Author Contributions

⊥Z.L. and X.H. contributed equally.

### Notes

The authors declare no competing financial interest.

## ■ ACKNOWLEDGMENTS

We are especially indebted to one of the reviewers for their exceptionally rigorous and insightful critique, which has been instrumental in enhancing the mechanistic foundation of this manuscript. Y.W. acknowledges the funding support from the National Natural Science Foundation of China (22250004 and 22572058), National Key R&D Program of China (2023YFA1509001), Guangdong Innovative and Entrepreneurial Research Team Program (2023ZT10C139), Guangzhou Basic and Applied Basic Research Foundation (2024D03J0007), and PCOSS Open Project (202202).

## ■ REFERENCES

(1) Deng, M.; Yu, J.; Blackmond, D. G. Symmetry breaking and chiral amplification in prebiotic ligation reactions. *Nature* **2024**, *626*, 1019−1024.
(2) Yu, J.; Darú, A.; Deng, M.; Blackmond, D. G. Prebiotic access to enantioenriched amino acids via peptide-mediated transamination reactions. *Proc. Natl. Acad. Sci. U.S.A.* **2024**, *121*, e2315447121.
(3) Ahrendt, K. A.; Borths, C. J.; MacMillan, D. W. C. New strategies for organic catalysis: the first highly enantioselective organocatalytic diels−alder reaction. *J. Am. Chem. Soc.* **2000**, *122*, 4243−4244.
(4) List, B.; Lerner, R. A.; Barbas, C. F. Proline-catalyzed direct asymmetric aldol reactions. *J. Am. Chem. Soc.* **2000**, *122*, 2395−2396.
(5) Han, B.; He, X. H.; Liu, Y. Q.; et al. Asymmetric organocatalysis: an enabling technology for medicinal chemistry. *Chem. Soc. Rev.* **2021**, *50*, 1522−1586.
(6) Pu, L. Enantioselective fluorescent recognition of free amino acids: challenges and opportunities. *Angew. Chem., Int. Ed.* **2020**, *59*, 21814−21828.
(7) Han, Z.; Wang, K.-Y.; Wang, M.; Shi, W. Indirect construction of chiral metal−organic frameworks for enantioselective luminescence sensing. *Acc. Chem. Res.* **2025**, *58*, 625−634.
(8) Wang, Y.; Zhang, X.; Xie, D.; et al. Chiral engineered biomaterials: new frontiers in cellular fate regulation for regenerative medicine. *Adv. Funct. Mater.* **2025**, *35*, 2419610.
(9) Knowles, W. S.; Sabacky, M. J. Catalytic asymmetric hydrogenation employing a soluble, optically active, rhodium complex. *Chem. Commun.* **1968**, 1445.
(10) Nozaki, H.; Takaya, H.; Moriuti, S.; Noyori, R. Homogeneous catalysis in the decomposition of diazo compounds by copper chelates. *Tetrahedron* **1968**, *24*, 3655−3669.
(11) Katsuki, T.; Sharpless, K. B. The first practical method for asymmetric epoxidation. *J. Am. Chem. Soc.* **1980**, *102*, 5974−5976.
(12) Zhang, L.; Meggers, E. Chiral-at-metal catalysts: history, terminology, design, synthesis, and applications. *Chem. Soc. Rev.* **2025**, *54*, 1986−2005.
(13) Wheeler, S. E.; Seguin, T. J.; Guan, Y.; Doney, A. C. Noncovalent interactions in organocatalysis and the prospect of computational catalyst design. *Acc. Chem. Res.* **2016**, *49*, 1061−1069.
(14) Yu, B.; Huang, Y.; Zhang, H.; Huang, H. Adaptive dynamic kinetic resolution enables alteration of chiral induction with ring sizes. *Nat. Chem.* **2025**, *17*, 1256.
(15) Chen, Y.-W.; Qiu, Y.; Liu, Y.; et al. Intermolecular asymmetric functionalization of unstrained C(sp3)−C(sp3) bonds in allylic substitution reactions. *Nat. Synth.* **2024**, *3*, 1011−1020.
(16) Guan, C.-Y.; Zou, S.; Luo, C.; et al. Catalytic asymmetric synthesis of planar-chiral dianthranilides via (dynamic) kinetic resolution. *Nat. Commun.* **2024**, *15*, No. 4580.
(17) Lam, Y.-h.; Grayson, M. N.; Holland, M. C.; Simon, A.; Houk, K. N. Theory and modeling of asymmetric catalytic reactions. *Acc. Chem. Res.* **2016**, *49*, 750−762.
(18) Li, B.; Xu, H.; Dang, Y.; Houk, K. N. Dispersion and steric effects on enantio-/diastereoselectivities in synergistic dual transition-metal catalysis. *J. Am. Chem. Soc.* **2022**, *144*, 1971−1985.
(19) Huffman, M. A.; Fryszkowska, A.; Alvizo, O.; et al. Design of an in vitro biocatalytic cascade for the manufacture of islatravir. *Science* **2019**, *366*, 1255−1259.
(20) Casamajo, A. R.; Yu, Y.; Schnepel, C.; et al. Biocatalysis in drug design: engineered reductive aminases (RedAms) are used to access chiral building blocks with multiple stereocenters. *J. Am. Chem. Soc.* **2023**, *145*, 22041−22046.
(21) Lister, T. M.; Roberts, G. W.; Hossack, E. J.; et al. Engineered enzymes for enantioselective nucleophilic aromatic substitutions. *Nature* **2025**, *639*, 375−381.
(22) De Graaf, F. V.; Zoister, C.; Schade, B.; et al. Amplification of asymmetry via structural transitions in supramolecular polymer−surfactant coassemblies. *J. Am. Chem. Soc.* **2025**, *147*, 17468−17476.
(23) Hou, B.; Wang, K.; Jiang, C.; et al. Homochiral covalent organic frameworks with superhelical nanostructures enable efficient chirality-induced spin selectivity. *Angew. Chem., Int. Ed.* **2024**, *63*, e202412380.
(24) Bi, Y.; Cheng, C.; Zhang, Z.; et al. Controlled hierarchical self-assembly of nanoparticles and chiral molecules into tubular nanocomposites. *J. Am. Chem. Soc.* **2023**, *145*, 8529−8539.
(25) Qiu, Y.; Wei, X.; Lam, J. W. Y.; Qiu, Z.; Tang, B. Z. Chiral nanostructures from artificial helical polymers: recent advances in synthesis, regulation, and functions. *ACS Nano* **2025**, *19*, 229−280.
(26) Zhao, Y.; Kawano, H.; Yamagishi, H.; et al. Pathway complexity in nanotubular supramolecular polymerization: metal−organic nanotubes with a planar-chiral monomer. *J. Am. Chem. Soc.* **2023**, *145*, 13920−13928.
(27) Weyandt, E.; Leanza, L.; Capelli, R.; et al. Controlling the length of porphyrin supramolecular polymers via coupled equilibria and dilution-induced supramolecular polymerization. *Nat. Commun.* **2022**, *13*, No. 248.
(28) Takahashi, S.; Abe, T.; Sato, H.; Hiraoka, S. Pathway bias and emergence of quasi-irreversibility in reversible reaction networks: extension of curtin-hammett principle. *Chem* **2023**, *9*, 2971−2982.
(29) Jansen, S. A. H.; Markvoort, A. J.; Graaf, F. V. d.; et al. Bayesian optimization for multicomponent supramolecular systems. *J. Am. Chem. Soc.* **2025**, *147*, 33607−33614.
(30) Wang, Y.; Lin, H. X.; Chen, L.; et al. What molecular assembly can learn from catalytic chemistry. *Chem. Soc. Rev.* **2014**, *43*, 399−411.
(31) Tateishi, T.; Takahashi, S.; Okazawa, A.; et al. Navigated self-assembly of a $Pd_2L_4$ cage by modulation of an energy landscape under kinetic control. *J. Am. Chem. Soc.* **2019**, *141*, 19669−19676.
(32) Wang, L.; Song, B.; Khalife, S.; et al. Introducing seven transition metal ions into terpyridine-based supramolecules: self-assembly and dynamic ligand exchange study. *J. Am. Chem. Soc.* **2020**, *142*, 1811−1821.
(33) Kulkarni, C.; Meijer, E. W.; Palmans, A. R. A. Cooperativity scale: a structure−mechanism correlation in the self-assembly of benzene-1,3,5-tricarboxamides. *Acc. Chem. Res.* **2017**, *50*, 1928−1936.
(34) d'Orchymont, F.; Holland, J. P. Cooperative capture synthesis of functionalized heterorotaxanes—chemical scope, kinetics, and mechanistic studies. *J. Am. Chem. Soc.* **2023**, *145*, 12894−12910.

(35) Ouyang, G.; Ji, L.; Jiang, Y.; Würthner, F.; Liu, M. Self-assembled möbius strips with controlled helicity. *Nat. Commun.* **2020**, *11*, No. 5910.
(36) Castilla, A. M.; Ousaka, N.; Bilbeisi, R. A.; et al. High-fidelity stereochemical memory in a $Fe_4^{II}L_4$ tetrahedral capsule. *J. Am. Chem. Soc.* **2013**, *135*, 17999−18006.
(37) Chen, Y.; Cao, Z.; Feng, T.; et al. Enantioselective self-assembly of a homochiral tetrahedral cage comprising only achiral precursors. *Angew. Chem., Int. Ed.* **2024**, *63*, e202400467.
(38) Zhou, Y.; Li, H.; Zhu, T.; Gao, T.; Yan, P. A highly luminescent chiral tetrahedral $Eu_4L_4(L')_4$ cage: chirality induction, chirality memory, and circularly polarized luminescence. *J. Am. Chem. Soc.* **2019**, *141*, 19634−19643.
(39) Wang, H.-X.; Zhu, X.; Liu, M. Emergent chiral and topological nanoarchitectonics in self-assembled supramolecular systems. *Chem. Soc. Rev.* **2025**, *54*, 5516−5550.
(40) Qu, H.; Shi, P.; Lei, Z. C.; et al. Some thoughts about controllable assembly (III): theoretical frameworks and physicochemical foundations of catassembly. *Sci. Sin. Chim.* **2025**, *55*, 1954−2003.
(41) Tian, Z.-Q.; Ding, S.; Fan, F.; et al. Some thoughts about controllable assembly (I): From catalysis to cassemblysis. *Sci. Sin. Chim.* **2012**, *42*, 525−547.
(42) Yang, L.; Wang, X.; Zhou, C.; et al. Some thoughts about controllable assembly (II): catassembly in living organism. *Sci. Sin. Chim.* **2020**, *50*, 1781−1800.
(43) Lei, Z.-C.; Wang, X.; Yang, L.; et al. What can molecular assembly learn from catalysed assembly in living organisms? *Chem. Soc. Rev.* **2024**, *53*, 1892−1914.
(44) Burke, M. J.; Nichol, G. S.; Lusby, P. J. Orthogonal selection and fixing of coordination self-assembly pathways for robust metallo-organic ensemble construction. *J. Am. Chem. Soc.* **2016**, *138*, 9308−9315.
(45) Saha, M. L.; Pramanik, S.; Schmittel, M. Spontaneous and catalytic fusion of supramolecules. *Chem. Commun.* **2012**, *48*, 9459.
(46) Prins, L. J.; De Jong, F.; Timmerman, P.; Reinhoudt, D. N. An enantiomerically pure hydrogen-bonded assembly. *Nature* **2000**, *408*, 181−184.
(47) Wang, Y.; Sun, Y.; Shi, P.; et al. Chaperone-like chiral cages for catalyzing enantio-selective supramolecular polymerization. *Chem. Sci.* **2019**, *10*, 8076−8082.
(48) Jouault, N.; Moulin, E.; Giuseppone, N.; Buhler, E. Light scattering strategy for the investigation of time-evolving heterogeneous supramolecular self-assemblies. *Phys. Rev. Lett.* **2015**, *115*, 085501.
(49) Ellis, T. K.; Galerne, M.; Armao, J. J.; et al. Supramolecular electropolymerization. *Angew. Chem., Int. Ed.* **2018**, *57*, 15749−15753.
(50) Zhao, J.-S.; Wang, J.-H.; He, W.-B.; Ruan, Y.-B.; Jiang, Y.-B. Isolable chiral aggregates of achiral $\pi$-conjugated carboxylic acids. *Chem. − Eur. J.* **2012**, *18*, 3631−3636.
(51) Jiao, Y.; Qiu, Y.; Zhang, L.; et al. Electron-catalysed molecular recognition. *Nature* **2022**, *603*, 265−270.
(52) Hu, J.; Tong, T.; Shi, P.; et al. Polymer-catalyzed DNA assembly relies on weak non-covalent interactions. *Cell Rep. Phys. Sci.* **2024**, *5*, 101937.
(53) Lei, Z.-C.; Yin, X.; Wang, X.; et al. RNA can function as molecular chaperone for RNA folding. *Giant* **2020**, *1*, 100008.
(54) Li, W.; Zhou, Y.; Zhang, X.; et al. Insights into the assembly of peptides catalyzed by polysaccharides. *J. Phys. Chem. B* **2025**, *129*, 487−495.
(55) Li, W.; Zhou, Y.; He, S.; et al. An artificial chaperone serves a dual role in regulating the assembly of peptides through phase separation. *Aggregate* **2024**, *5*, e496.
(56) Sun, Y.; Fang, Y.; Liu, Y.; et al. Designing catalysts to accelerate a protein−peptide assembly-reaction cascade. *ACS Cent. Sci.* **2025**, *11*, 1166.
(57) Qu, H.; Wang, Y.; Li, Z.; et al. Molecular face-rotating cube with emergent chiral and fluorescence properties. *J. Am. Chem. Soc.* **2017**, *139*, 18142−18145.
(58) Korevaar, P. A.; George, S. J.; Markvoort, A. J.; et al. Pathway complexity in supramolecular polymerization. *Nature* **2012**, *481*, 492−496.
(59) Blow, D. M.; Smith, J. M. Enzyme substrate and inhibitor interactions. *Philos. Trans. R. Soc. B: Biol. Sci.* **1975**, *272*, 87−97.
(60) Pedregosa, F.; et al. Scikit-learn: Machine learning in Python. *J. Mach. Learn. Res.* **2011**, *12*, 2825−2830.
(61) Attias, H. A Variational Baysian Framework for Graphical Models. In *Advances in Neural Information and Processing Systems*; MIT Press, 1999; Vol. *12*.
(62) Blei, D. M.; Jordan, M. I. Variational inference for Dirichlet process mixtures. *Bayesian Anal.* **2006**, *1*, 121−143.
(63) Rasmussen, C. E.; Williams, C. K. I. *Gaussian Processes for Machine Learning*; MIT Press, 2005.
(64) Rong, Y.; Chen, P.; Liu, M. Self-assembly of water-soluble tpps in organic solvents: from nanofibers to mirror imaged chiral nanorods. *Chem. Commun.* **2013**, *49*, 10498−10500.




https://doi.org/10.1021/jacs.5c16840
J. Am. Chem. Soc. XXXX, XXX, XXX−XXX